THESIS FOR THE DEGREE OF LICENTIATE OF ENGINEERING

Characterization of WC-Co tools used for machining of Alloy 718 under the influence of high-pressure coolant supply

Philipp Hoier

Department of Industrial and Materials Science

CHALMERS UNIVERSITY OF TECHNOLOGY

Gothenburg, Sweden 2017

Characterization of WC-Co tools used for machining of Alloy 718 under the influence of high-pressure coolant supply

PHILIPP HOIER

Technical report no IMS-2017-2
Department of Industrial and Materials Science
Chalmers University of Technology
SE-412 96 Gothenburg
Sweden
Telephone + 46 (0)31-772 1000

Printed by Chalmers Reproservice
Gothenburg, Sweden 2017

Characterization of WC-Co tools used for machining of Alloy 718 under the influence of high-pressure coolant supply

PHILIPP HOIER

Department of Industrial and Materials Science
Chalmers University of Technology

Abstract

The use of high-pressure jets for supply of coolant to the cutting zone has the potential to significantly increase the productivity and process stability when machining difficult-to-cut materials such as Ni-based superalloys. Apart from better chip-breakability, the jets enable the coolant to reach closer to the cutting edge and hence enhance its capability to dissipate heat.

This work deals with characterization of conventional and surface-modified uncoated WC-Co tools used for machining of a Ni-based superalloy (Alloy 718) with assistance of high-pressure coolant supply. Specifically, scanning electron microscopy (SEM) together with energy-dispersive X-ray spectroscopy (EDX) were used to study the flank wear lands and areas impinged by the coolant of conventional and surface-modified tools.

As compared to conventional tools, the surface-modified tools (with arrays of square pyramidal shaped dimples on rake and flank faces) enabled to reduce flank wear. This was linked to the larger surface area provided by the modifications which can enhance the tool-coolant interaction. In that way, the heat dissipation during cutting is improved and the tool is subjected to less thermal softening and wear.

At the tool surfaces, the Co-binder was removed by erosion during the coolant-impact when machining. The erosion occurred on areas of both rake and flank surface which are impinged by the high-pressure coolant jets and are not in contact with the workpiece during cutting. The erosion damage can be used to determine the access of coolant to the cutting edge. Such observations are not possible during the machining since the cutting zone is visually inaccessible. In addition, the existence of an erosion-free zone adjacent to the flank wear land was observed. This indicated that the coolant jets did not reach this location. Instead, the high temperature occurring at the tool surface during machining led to vaporization of the coolant and the formed vapor-barrier prevented the coolant to reach closer to the cutting zone.

After the conducted machining tests, the worn flank faces were covered by workpiece material. Removal of the adhered material allowed to characterize the underlying tool microstructure. However, fragments of workpiece precipitates were still found on the worn tool surface. Because of longer contact times and larger thermal loads in the tertiary shearing zone in connection with increasing flank wear, the morphology of the fragments changed to a more smeared-out appearance.

Keywords: High-pressure coolant supply, tool wear, surface-modifications, vapor-barrier, Alloy 718, erosion

Preface

This licentiate thesis is based on the work which was performed at the Department of Materials and Manufacturing Technology between September 2014 and April 2017 under supervision of Professor Uta Klement. (Notice that the department changed name on May 1st 2017) The work was co-supervised by Professor Tomas Beno, University West, Trollhättan, and carried out with financial support from Västra Götalandsregionen, Sweden, within the PROSAM project. The machining experiments were performed in close collaboration with Nageswaran Tamil Alagan who was the "twin PhD student" in this project. The thesis consists of an introduction and the following appended papers:

Paper 1: Characterization of tool wear when machining Alloy 718 with high pressure cooling using conventional and surface-modified WC-Co tools
P. Hoier, U. Klement, N.T. Alagan, T. Beno, A. Wretland
Conference Proceedings of the 7th International Swedish Production Symposium, 2016.
To be published in Journal of Superhard Materials

Paper 2: Co-erosion and localization of the vapor barrier in high-pressure jet assisted machining with uncoated WC-Co tools
P. Hoier, U. Klement, N.T. Alagan, T. Beno, A. Wretland
In manuscript

Paper 3: Flank wear characteristics of WC-Co tools when turning Alloy 718 with high-pressure coolant supply
P. Hoier, U. Klement, N.T. Alagan, T. Beno, A. Wretland
In manuscript

Contribution to the appended papers

Paper 1: I conducted all the characterization work and wrote the paper in collaboration with the co-authors. The tool modifications were designed by Nageswaran Tamil Alagan at University West.

Paper 2: I was involved in planning and conducting the experiments together with the co-authors and Andreas Lindgren at GKN Aerospace. The characterization was performed by me and the manuscript was written in collaboration with the co-authors.

Paper 3: I was involved in planning and conducting the experiments in collaboration with the co-authors and Andreas Lindgren at GKN Aerospace. White-light interferometry measurements were done with help of Amogh Vedantha Krishna at Halmstad University. All other characterization work was done by me. The manuscript was written in collaboration with the co-authors.

Table of Contents

1 Introduction

1.1 Background

Commercial aviation industry has seen a remarkable growth within the latest decades, reaching a staggering amount of 3.7 billion passenger departures in 2016 [1]. For 2017, a growth to almost 4 billion passenger departures is expected [1]. The increased demand for air travels is reflected in the higher number of new aircrafts delivered to airlines (Figure 1). For 2016 alone, an estimated 1700 new aircrafts have been delivered [1]. In their long term market outlook, Boeing estimates demand to over 39600 new airplanes in the next 20 years [2].

The increase in demand is mainly owing to the possibility of offering increasingly cheap flight fares. A major factor regarding costs is the fuel efficiency of aircrafts [1].

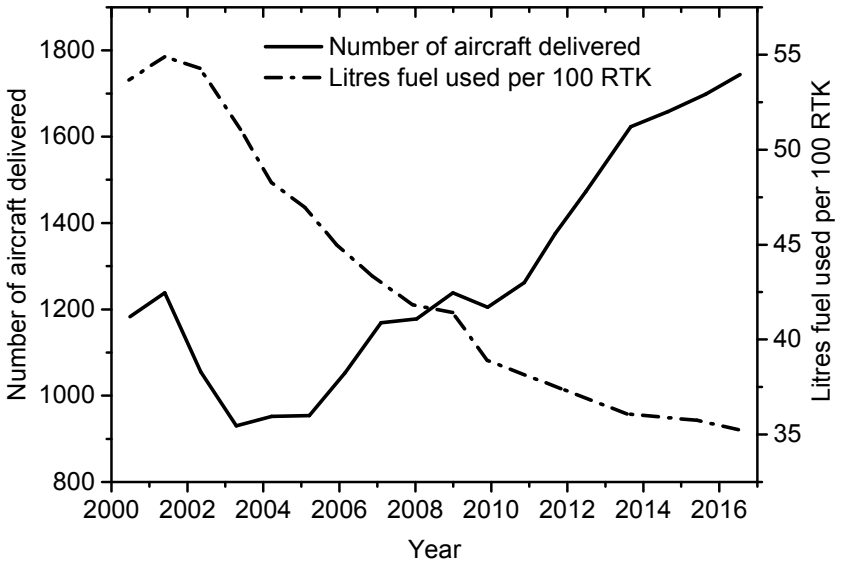

Figure 1: Recent development and forecast of average fuel consumption and aircraft deliveries to airlines worldwide. RTK = revenue tonne kilometer. Figure recreated from [1].

A key event in the past 50 years was the introduction and development of Ni-based superalloys [3]. This material class can be applied in the hot section of aircraft engines where it enables a continuous raise of operational temperature and hence engine efficiency [4].

However, processing of superalloys by means of machining operations is characterized by built-up of high temperatures in the cutting zone which is related to the material's high-temperature properties. High thermal loads on the tools lead to high wear rates and low applicable cutting speeds and feed rates which ultimately yield in high production costs.

During manufacture of typical engine components, up to 80% of the initial weight of a forging is removed by machining before the final shape of the component is attained [5]. Optimization of the cutting process and lowering the production costs is hence a key factor to meet the increasing demand on jet engines in an economical and sustainable way.

In that context, supply of coolant into the cutting zone by high-pressure jets has shown to be able to lower the thermal loads on the cutting tools during machining. As a consequence, enhanced productivity by longer tool life or higher cutting speed and feed rate can be achieved.

1.2 Research objective

The fundamental mechanisms of how the coolant jets affect the cutting process are often based on hypotheses which are not verified as the cutting zone is inaccessible during the actual machining. Post-test material characterization is one way of obtaining information about wear-related microstructural changes.

In the present work, uncoated WC-Co tools used for machining of Alloy 718 under the influence of high-pressure coolant supply were characterized.

The objectives can be formulated as the following:

- Comparison of conventional tools with surface-modified tools with respect to their wear behavior.
- Analysis of the coolant impingement on the tool surface and access of the coolant to the cutting edge during machining.
- Characterization of the wear characteristics resulting from the sliding contact between workpiece and tool in the tertiary shearing zone.

2 Workpiece and tool material

2.1 Ni-based superalloys and their machinability

Ni-based superalloys are complex engineering materials consisting of many alloying elements (usually up to ten) with Ni as the major constituent. The microstructure is dictated by the chemical composition as well as the thermo-mechanical processing steps and typically consists of a combination of some of the following phases [6], [7]:

Gamma phase (γ)
Matrix with face-centered cubic (FCC) structure consisting of mainly Ni with other alloying elements in solid solution.

Gamma prime precipitates (γ′)
Intermetallic phase with FCC structure, consisting of Ni_3X (X: e.g. Al or Ti).

Gamma double prime precipitates (γ′′)
Intermetallic phase with thermodynamically metastable body-centered tetragonal structure (BCT), consisting of Ni_3Nb.

Delta phase (δ)
Intermetallic phase with thermodynamically stable orthorhombic structure, it is the stable form of γ′′ (Ni_3Nb).

Carbides
Mainly of type MC, M_6C, and $M_{23}C_6$ (M: e.g. Nb or Ti).

Laves phase
Intermetallic phase with hexagonal structure (HCP), general formula $(Fe,Cr,Mn,Si)_2(Mo,Ti,Nb)$ [8].

A combination of solid solution strengthening and precipitation hardening (mostly by γ′ and γ′′) provides superalloys with both high tensile strength and creep resistance at high temperatures. Furthermore, additions of Cr offer corrosion and oxidation resistance [7].

The tensile strength of a superalloy as compared with a common steel as a function of temperature is shown in Figure 2. As can be seen, the tensile strength of the superalloy exceeds the steel throughout the whole temperature range. Table 1 provides additional physical and mechanical properties of these two alloys. Evidentially, the above described metallurgy of superalloys provides advantageous mechanical properties for application at high temperature.

It is these properties that make superalloys the foremost important class of materials used in and around the combustion chamber of aircraft engines, contributing about 50% to the total weight of a jet engine of a modern commercial airplane [3].

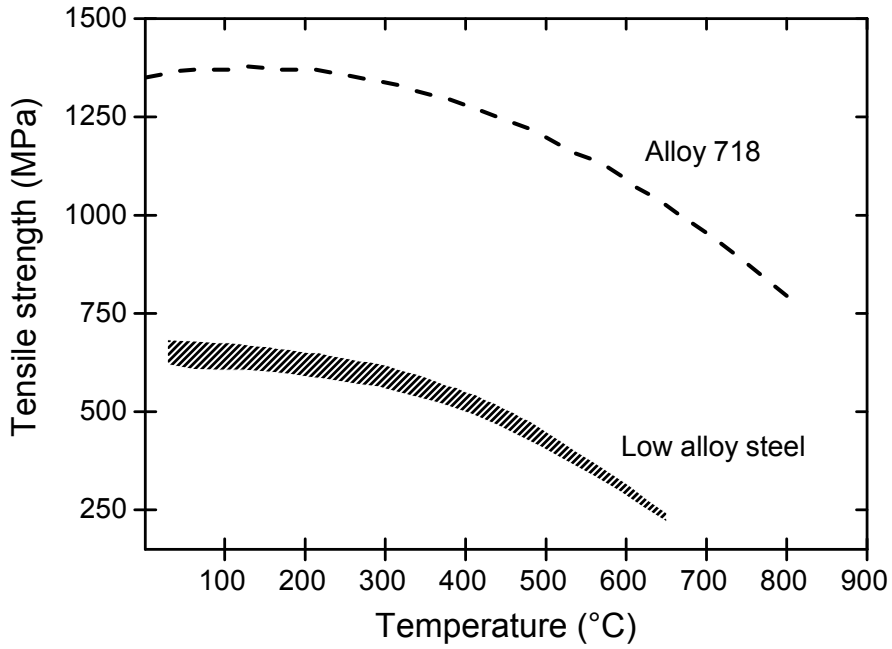

Figure 2: Comparison of tensile strength of a superalloy (Alloy 718) with a low alloy steel (AISI 4130). Drawn with data taken from [9].

Table 1: Physical and mechanical properties of AISI 4130 low alloy steel as compared to Alloy 718 superalloy. Material data taken from [9].

	Low alloy steel, AISI 4130 (normalized)	Alloy 718 (solutionized)
Thermal conductivity [W/(m×°C)]	41.5-45	11.6-12.6
Young's modulus [GPa]	208-216	203-213
Yield strength [MPa]	325-405	724-800
Elongation to fracture [%]	18-29	35-50

During manufacturing by metal cutting, the characteristic properties of superalloys give rise to major challenges [10], [11]. Especially, the ability to maintain strength at high temperature (Figure 2) together with the low thermal conductivity (Table 1) lead to high thermal and mechanical loads on the cutting tools. The high loads are further enhanced by the tendency of superalloys to strain harden.

Another issue is the high ductility (elongation to fracture) of superalloys which favors the generation of continuous chips. They can hit and damage the tool and the generated surfaces, hence, negatively affect the surface integrity [12].

Due to the mentioned challenges with machining of superalloys, the cutting tool materials have to have high wear resistance, high toughness, and high hardness together with chemical stability at elevated temperatures.

2.2 Cemented tungsten carbides (WC-Co)

Cemented tungsten carbide is a composite material, which is produced by powder metallurgy using liquid phase sintering. It combines the hardness and wear resistance of tungsten carbide (WC) grains with the toughness of a ductile binder phase (most commonly Co) [13].

Since its introduction and first application in the 1920s, WC-Co has become one of the most common materials for applications requiring wear resistance like tools in manufacturing industry [14]. In metal cutting, applications include machining of cast iron, non-ferrous materials, and heat resistant materials [15].

The typical microstructure of sintered WC-Co can be seen in Figure 3. An interconnected skeleton of WC grains (bright) within the Co-binder (dark) is visible. The crystal structure of WC is HCP with polar crystal planes which results in a flat, truncated triangular prism as the equilibrium shape of individual WC crystals [16]. This explains the shape of WC grains seen in Figure 3.

Figure 3: The general microstructure of WC-Co seen in cross-section with an interconnected skeleton of WC grains (bright) and Co-binder (dark) in-between.

During sintering, WC partially dissolves in the liquid Co-binder and re-precipitates during cooling with some WC staying in solid solution even at room temperature [17], [18].

WC-Co usually contains about 4 to 12 wt.% Co-binder and the size of WC grains is commonly in the range of 0.5 to 10 µm [19]. Adjustment of mechanical properties of WC-Co based cemented carbides is mostly done by changing WC grain size and binder content as well as by addition of other refractory carbides (e.g. TaC, NbC, or TiC). In this way the most suitable

combination of hardness, transverse rupture strength, and fracture toughness with respect to the specific application can be achieved [20].

3 Theory of turning

Turning belongs to the group of metal cutting operations. In metal cutting, material is removed from a workpiece in form of chips in order for the workpiece to attain a desired shape [19]. In turning, the workpiece is clamped in a rotating chuck and the tool is fed into the workpiece as exemplified in Figure 4. Here, a face turning operation is shown where the tool is moving in radial direction towards the center of the workpiece. By combining many turning operations involving different tool holders and tool types, components of complex geometry can be manufactured.

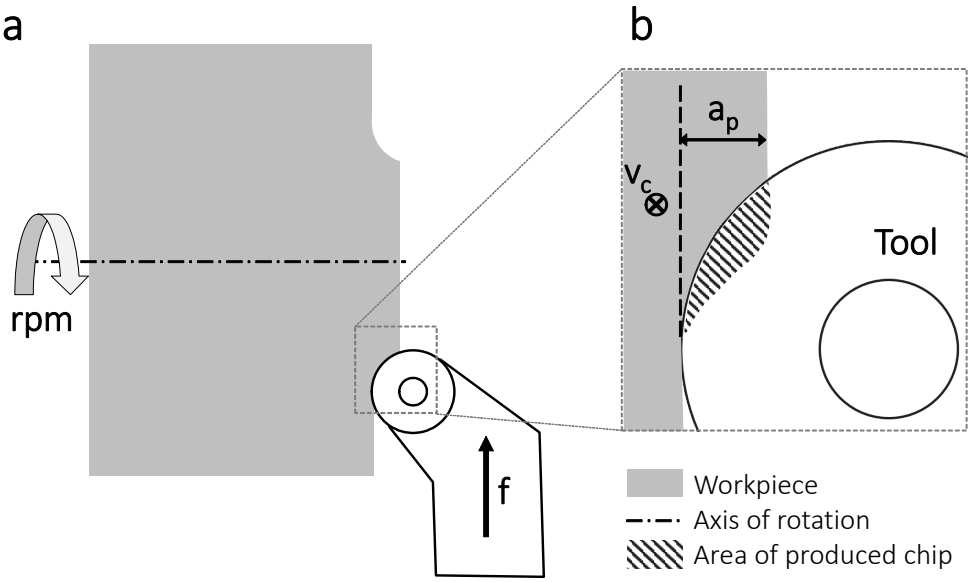

Figure 4: Schematic of the face turning process: Feed rate (f) in radial direction, cutting speed (v_c) pointing inward the imaged plane, and depth of cut (a_p) are indicated.

3.1 The cutting zone

The cross-sectional view through the contact zone between workpiece, tool, and generated chip are shown schematically in Figure 5. Shearing of workpiece material and subsequent removal in form of chips occurs due to the relative motion between the wedge-shaped tool and the workpiece (indicated by cutting speed v_c).

Figure 5a shows the forces acting on the tool. Indicated are also rake and flank face, i.e. the tool sides facing the chip and generated workpiece surface, respectively.

During cutting, almost all of the used mechanical work is converted into heat. This occurs in the primary (I), secondary (II), and tertiary (III) shearing zones [15], illustrated in Figure 5b. Here, the workpiece is undergoing shear strains reaching up to 4 and over 20 in the primary and secondary shearing zone, respectively [19]. The high shear strains together with high strain rates of up to 10^6 1/s can lead to tool surface temperatures exceeding 1000 °C [15].

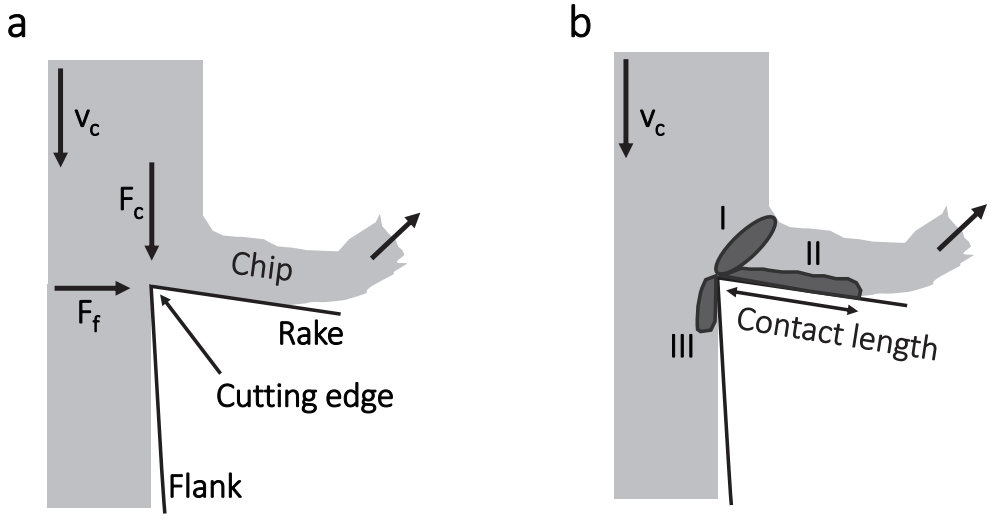

Figure 5: Schematics of the chip formation process in the cutting zone: (a) Cutting force (F_c) and feed force (F_f) are indicated; (b) the three shearing zones (I-III) are shown.

3.2 Forms of tool wear

In general, wear can be defined as mechanically induced removal of material from a solid surface [21]. In metal cutting, tool wear occurs from the mechanical and thermal loads the tool is subjected to due to its sliding contact with the workpiece. Two of the most common wear forms are flank wear (VB) and crater wear (KT) as seen in Figure 6.

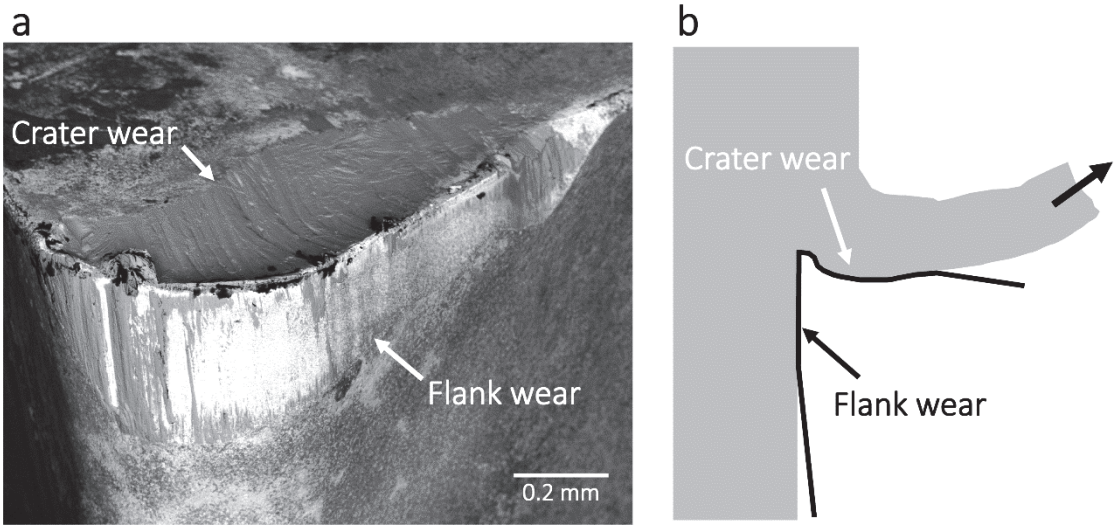

Figure 6: Commonly observed wear forms in metal cutting: (a) SEM micrograph of a worn cutting edge exhibiting crater and flank wear. (b) Illustration of crater and flank wear on worn cutting tool in cross-section.

Progressing flank wear leads to an increased contact area between the tool flank and the generated workpiece-surface. As a direct consequence, the feed force and shear force acting on the flank face increase. Furthermore, increased friction and shearing in the tertiary shearing zone lead to a temperature rise in the cutting zone [19], [22].

Crater wear occurs in the contact zone between chip and rake. With its progression, the load-bearing capability of the cutting edge decreases and the tool becomes more prone for sudden catastrophic failure [22].

Flank wear and crater wear are gradually developing forms of wear. Plastic deformation and chipping of the cutting edge, however, are generally sudden tool failure modes and are caused by exceedingly high mechanical and thermal loads acting on the tool.

In general, tool wear negatively affects the dimensional accuracy and functional properties of produced component surfaces. In order to meet set requirements, it is therefore necessary to replace worn tools with new tools as soon as a certain specified wear is reached [19]. In practice, a certain maximum flank wear land (VB_{max}) is often set as the wear criterion [22].

3.3 Tool wear mechanisms in metal cutting

This chapter will introduce some of the mechanisms occurring at the workpiece/tool interface in connection with the cutting process which are responsible for the gradual loss of tool material. Schematics of the respective mechanisms are presented in Figure 7.

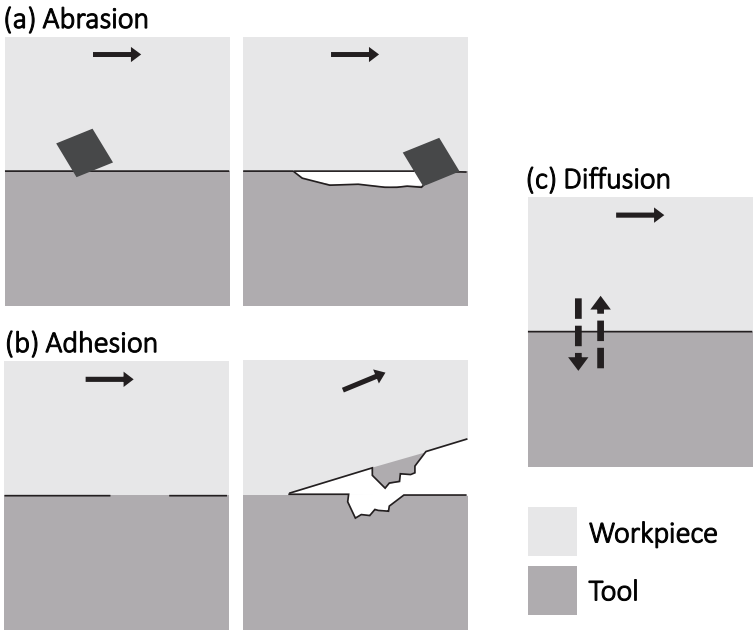

Figure 7: Illustrations of tool wear mechanisms occurring during metal cutting.

Abrasive wear

Abrasion is caused by hard particles cutting or ploughing into the tool due to their ability to penetrate the tool surface during relative tangential movement. The hard particles can originate from the workpiece (e.g. precipitates, carbides, inclusions) or from the tool by breaking-off and then slide along the tool surface [15].

Adhesive wear

The workpiece/tool interface in the cutting zone is characterized by very high contact pressures. Consequently, the real area of contact constitutes a large portion of the apparent contact area between the tool and the workpiece [19]. This tight tool-workpiece contact in the cutting zone promotes the formation of micro-welds between the mating materials. During relative tangential

movement between tool and workpiece, material-separation occurs in the tool rather than at the interface between tool and workpiece. In that case, part of the tool material is pulled out and subsequently removed [15].

Diffusion and dissolution

During cutting, the tool is in constant contact with a freshly generated workpiece surface. The mating surfaces are inaccessible for oxygen and other reactive species. Therefore, no oxide layer or other adsorbed layer can form at the interface between tool and workpiece. At high temperature and pressure, the conditions at the tool-workpiece interface in the cutting zone can give rise to diffusion processes [19].

One possible mechanism is that atoms of the tool material diffuse into the workpiece and/or chip which leads to direct loss of material from the tool [19]. Alternatively, diffusion of atoms from the workpiece into the tool material can impair the material's wear resistance and hence lead to increased wear rate [23].

Plastic deformation

Excessive generation of heat during cutting can lead to softening of the tool material. If the tool is not able to withstand the mechanical loads any more, it deforms plastically. In case of WC-Co based cutting tools, the most common deformation mechanisms are: Plastic deformation of the Co-binder [18], plastic deformation of WC grains [24], and plastic deformation of the WC skeleton [25].

Relative importance of wear mechanisms

Usually, several of the wear mechanisms described above are active simultaneously. The relative importance of the individual mechanisms is depending on the temperature in the cutting zone [15]. In Figure 8, the contributions of the individual wear mechanisms to the overall wear rate are illustrated as a function of cutting temperature. As can be seen, adhesion is mostly active at relatively low cutting temperatures. Diffusion wear, however, is a thermally activated process and therefore only relevant at high cutting temperatures. Abrasion is an active mechanisms throughout the whole range of cutting temperatures.

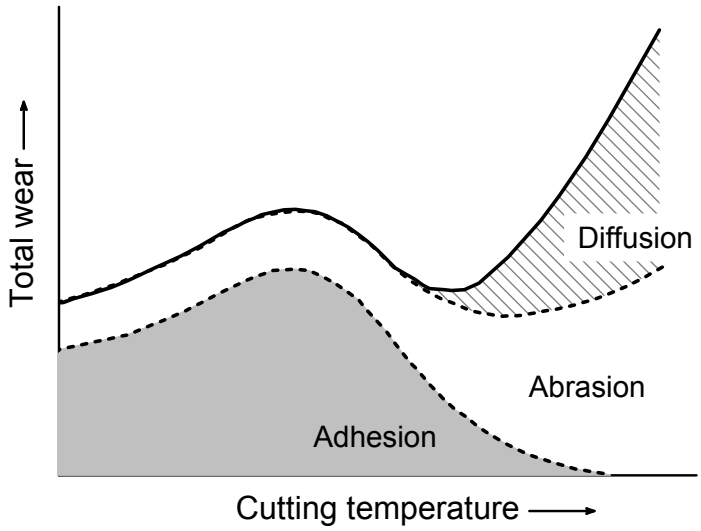

Figure 8: Importance of different wear mechanisms for tool wear with increasing cutting temperature (by e.g. increasing cutting speed or feed rate). Adapted and modified from [15].

4 High-pressure jet assisted machining

Due to the high thermo-mechanical loads on cutting tools when machining superalloys (described in Chapter 2.1), it is common practice to apply coolants to the cutting zone [12]. The beneficial effect of coolants during machining is attributed to their ability to dissipate heat from the cutting zone as well as to provide lubrication to the tool-workpiece contact zones.

In industry, the most common method of supplying coolant to the cutting zone is flood cooling [12]. Despite its common application, flood cooling has some drawbacks. Namely, the coolant is applied in rather uncontrolled manner and mainly hits the chip-top side. The zones of highest friction and heat around the shearing zones are therefore often not reached by the coolant and hence no effective cooling can be achieved [10].

A more effective use of coolant can be achieved by supplying coolant in form of high-pressure jets to the tool rake or flank face. In that way, the contact zones of the tool with the chip (rake) and with the generated workpiece surface (flank) can specifically be targeted. Especially in connection to difficult-to-cut materials, this technology can lead to a substantial increase in productivity and process stability [12].

4.1 Summary of previous work

In the first study regarding high-pressure jet assisted machining in 1952, Pigott and Coldwell [26] applied flank-sided cooling at 2.8 MPa pressure. They reported an increase of tool life of up to seven to eight times as compared to conventional cooling when machining steel.

Since then, an increasing amount of studies have been published investigating the influence of the coolant jet parameters (supply pressure (p) and flow rate (Q)) on the tool life, cutting temperature, and characteristics of chip formation in machining different materials. In this chapter, only publications dealing with high-pressure coolant supply in machining Alloy 718, the by far most used superalloy, are summarized.

Ezugwu et al. [27] have investigated rake-sided high-pressure coolant supply with pressures of 11 to 20.3 MPa and flow rates of 20 to 50 l/min in rough turning (v_c = 20 - 50 m/min, f = 0.25 - 0.3 mm/rev, a_p = 2.5 - 3 mm) with PVD coated WC-Co tools. It was found that increasing coolant pressure leads to longer tool life. For the most aggressive cutting parameters, i.e. cutting speed of 50 m/min and feed rate of 0.3 mm/rev, a tool life increase of up to 740% was achieved when using the maximum pressure of 20.3 MPa.

In another study by Ezugwu et al. [28], the same coolant supply method and pressures were tested in connection with finish turning (v_c = 30 - 60 m/min, f = 0.1 - 0.2 mm/rev, a_p = 0.5 mm) using PVD coated WC-Co tools. A gain in tool life of up to 350% was established for the most severe cutting conditions. There was also evidence that there is an optimum coolant supply pressure at which the maximum tool life can be achieved. Increasing the coolant pressure beyond this critical pressure was seen to be detrimental for tool life [28].

In both publications [27], [28], the authors state that the positive effect of the high-pressure coolant jets is due to their increased access to the cutting edge which increases their effect on the chip-rake contact zone. Lower cutting temperatures then led to reduction of thermally related wear mechanisms and hence reduction of the overall wear rate.

Sharman et al. [29] investigated rake and/or flank-sided coolant supply with pressures of 0.5 to 45 MPa and a flow rate of 25 l/min in finish turning (v_c = 40 - 80 m/min, f = 0.35 mm/rev, a_p = 0.25 mm) with coated WC-Co tools. In contrast to other studies, no significant improvement with respect to tool life was achieved by use of high-pressure coolant supply. With the employed finishing conditions, the authors assumed that the temperature generated in the cutting zone was not high enough to benefit from the higher coolant supply pressures.

Courbon et al. [30] have conducted a systematic study on rough turning (v_c = 46 - 74 m/min, f = 0.2 - 0.25 mm/rev, a_p = 2 mm) with coated WC-Co tools. They varied the coolant supply pressure to the rake face from 50 to 130 MPa and the diameter of the nozzle from 0.25 to 0.4 mm (Q < 6 l/min). They concluded that by adjusting all relevant parameters regarding the coolant jets and the cutting parameters, the range of operability of the investigated tool can be extended by use of high-pressure cooling. Furthermore, temperature measurements showed that varying the parameters of the high-pressure jets did not have a significant influence on the thermal load on the tool [30]. In comparison to conventional cooling, however, a temperature decrease of 30% was achieved.

Similar results were presented by Klocke et al. [31] who reported up to 30% (200 °C) reduction of tool temperature as compared to conventional coolant supply. In their study, turning at semi-roughing conditions (v_c = 35 - 60 m/min, f = 0.2 mm/rev, a_p = 1 mm) was conducted with coated WC-Co tools. The coolant supply pressure was varied between 7 and 30 MPa with flow rates between 16 and 31 l/min.

In additions to the above mentioned effects, all the presented studies have in common that they reported a beneficial influence of rake-sided high-pressure cooling on the chip breakability. As a result, significantly shorter chips can be achieved which increases process safety.

4.2 Underlying effects of high-pressure coolant supply

Even though many studies have shown the beneficial influence of high-pressure coolant jets, only few are addressing the underlying mechanisms of how exactly the high-pressure jets affect the cutting process. Furthermore, the proposed mechanisms are mostly based on theories and assumptions without providing direct evidence.

Sangermann et al. [32] proposed that the temperature reduction associated with high-pressure coolant jets is due to a combination of mechanical, tribological, and thermal effects (see Figure 9).

First of all, precise targeting of the contact zones of the tool with the chip and workpiece enables the coolant to reach these zones more effectively which provides enhanced cooling and lubrication (thermal and tribological effect) [32].

The mechanical influence in rake-sided cooling is due to the high-pressure coolant jets' impact on the chip underside which exerts a force on the chip. Consequently, the chip is subjected to increased curl up and its contact length with the tool is decreased [33]. Hence, less frictional heat is generated and in addition the coolant can reach closer towards the cutting edge [34].

The coolant's access to the cutting zone is also enhanced by the jets' mechanical effect on the vapor barrier (rake- and flank-sided cooling). The formation of a vapor barrier on tool surfaces

during machining has been proposed regarding conventional or low pressure coolant supply [10], [35]–[37].

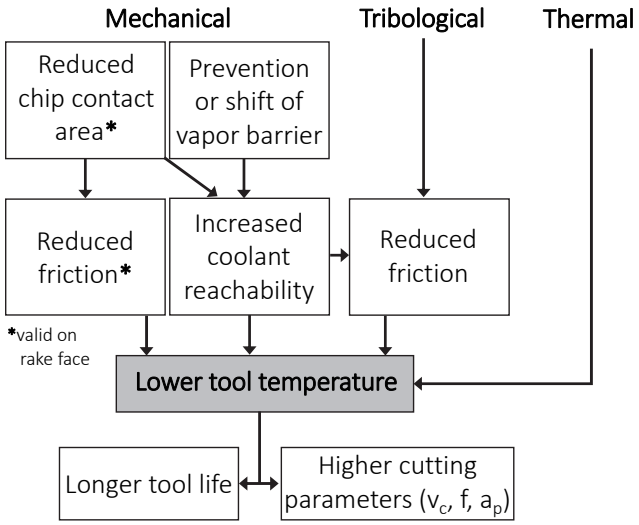

Figure 9: Summary of reported effects that high-pressure coolant supply has in the cutting zone (effects on chip-breakability are not included). Adopted and modified from [32].

Coolant-vaporization can be expected to occur upon contact with the hot tool surfaces during cutting. This can lead to formation of a vapor film hindering coolant from reaching the tool surface and hence the cutting zone. High-pressure coolant jets can either shift the location of the vapor barrier or prevent the initial formation which again facilitates the coolant's access to the cutting zone.

Based on results from Sørby et al. [37] and Klocke et al. [31], the interaction of a coolant jet with a film of vapor that has formed on the hot tool surface is shown schematically in Figure 10a. The vapor pressure of the boiling coolant (p_v) opposes the pressure of the coolant jet (p_{Jet}) at the coolant-vapor interface. In order to avoid the formation of a vapor barrier, it is therefore necessary that the coolant pressure is higher than the vapor pressure at the present temperature [37]. The dependency of pure water vapor pressure on temperature is shown in Figure 10b. As can be seen, the vapor pressure increases with temperature.

When neglecting the pressure drop that a jet of liquid (here coolant) is subjected to while propagating in air [32], [38], [39], the minimum required coolant supply pressure for avoidance of vapor can be estimated. Accordingly, the required coolant pressure (as measured at the nozzle) increases from about 4 MPa to about 17.5 MPa when the tool surface temperature rises from 250 °C to 350 °C.

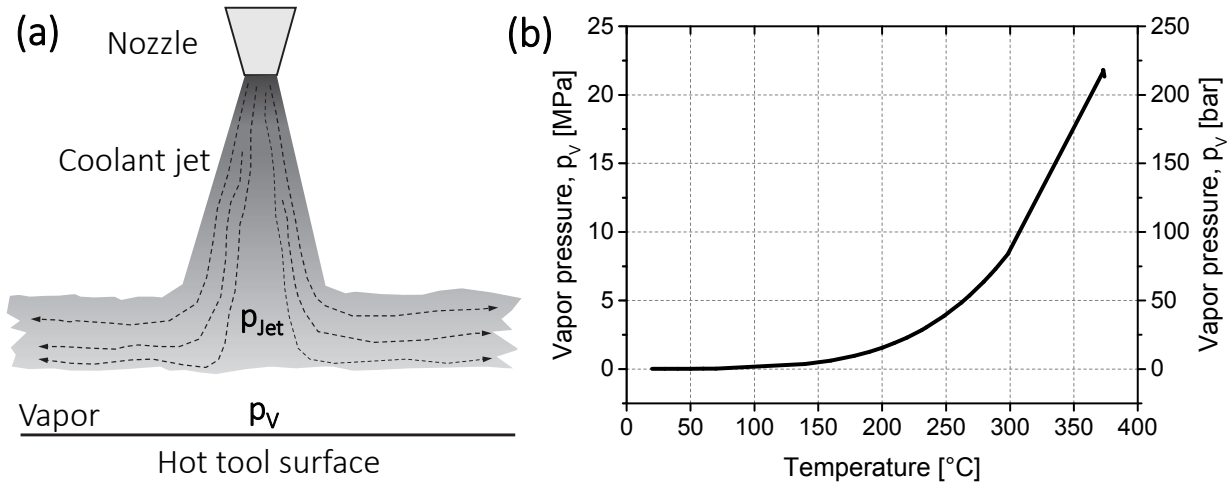

Figure 10: (a) Schematic of the vapor barrier phenomenon occurring upon coolant-tool contact. (b) Influence of temperature on vapor pressure of pure water. Drawn with data taken from [40].

5 Application of textured and surface-modified tools in metal cutting

It has been shown that texturing the surfaces of cutting tools can have a beneficial influence on the tribological properties when cutting different types of materials.

So far, most research has focused on textures applied to rake faces when cutting a variety of materials [41]–[47].

For example, Sugihara et al. [42], [46] have investigated arrays of grooves (100-150 nm deep and 700 nm apart) when milling an Al alloy under presence of coolant (Flow rate: 12.6 l/min, supply pressure not specified). They reported a significant decrease of adhesion of chips to the rake. Similar results were obtained by Obikawa et al. [44] who applied arrays of grooves and ridges (25 or 50 µm wide and 0.5, 1.0, and 1.2 µm deep/high, respectively) for turning an Al alloy under wet condition (no details about coolant supply provided).

Apart from reduced cutting forces, a reduction of wear was observed by Chang et al. [43] who used rake-textures (micro-scale grooves) on micro-milling cutters. The grooves were 4.5 µm wide, 300 µm long and 7.5 µm deep with a spacing of 4.5 µm between them. The machined workpiece was mold steel under the presence of coolant (supply method not specified).

In most of these studies, the positive effect of the surface textures was attributed to their interaction with the cutting fluid during machining. Specifically, surface textures can act as reservoirs for cutting fluid and increase the fluid's retention on the tool surface leading to enhanced lubrication and cooling. Evidentially, the cutting fluid and its supply-method plays a crucial role. In all mentioned studies with surface textures conventional flood cooling methods were applied and supply pressures, flow rates, types of nozzles etc. were described only vaguely.

In light of the positive effect of high-pressure coolant supply that has been summarized in Chapter 4, a combination of both technologies (tool textures and high-pressure coolant supply) has potential for enhancing the cutting performance further.

This is especially of interest in machining difficult-to-cut materials which are usually characterized by high temperatures in the cutting zone.

6 Experiments and methods of characterization

6.1 High-pressure jet assisted turning tests

All face turning experiments were carried out with a 5-axis CNC machine with a tool holder capable of supplying coolant to rake- and flank-side of the tool (see Figure 11). The coolant (5% emulsion) was supplied by a high-pressure pump at 16 MPa and 8 MPa pressure to rake and flank face of the tools, respectively. The coolant flow rates were 11.33 and 12.02 l/min through orifices of 0.8 and 1.2 mm diameter for rake and flank cooling, respectively.

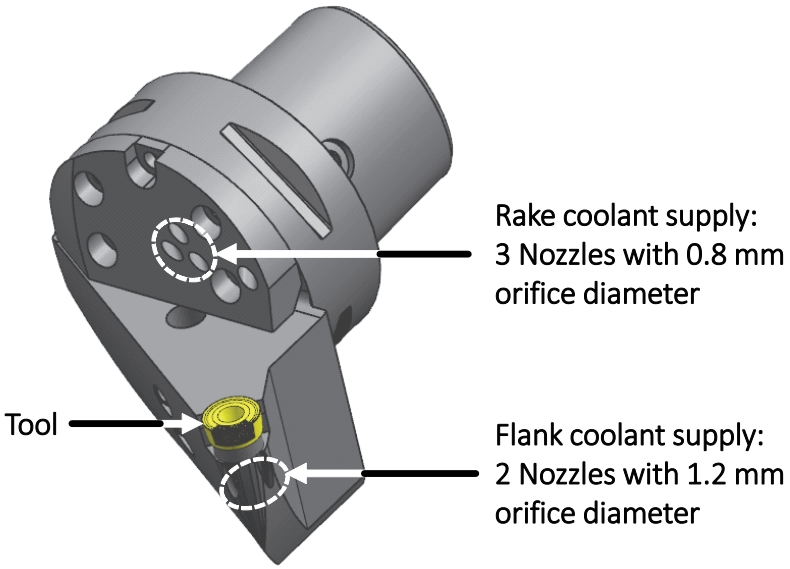

Figure 11: Tool holder with nozzles for high-pressure coolant supply used in this study (Image courtesy of Nageswaran Tamil Alagan, University West).

The workpiece was cast Alloy 718 with an average hardness of 381 ± 22 HV10. The face turning tests were conducted on rings with dimensions as seen in Figure 12. Calculation of spiral cutting lengths (SCL) corresponding to the tests was done using Eq. (1). D_1, D_m, and l_m correspond to the dimensions seen in Figure 12b. The cutting times T_C were calculated using Eq. (2).

In Table 2, all conducted tests are summarized. Aim of the first study (results are presented in Paper 1) was to determine the influence of tool surface modifications on the tool wear behavior. Therefore, two tests were conducted at the same cutting conditions and spiral cutting length using a conventional and a surface-modified tool. Additionally, a surface modified tool was tested at a higher cutting speed and feed rate.

In the second study (results are presented in Papers 2 and 3), the influence of spiral cutting length on the flank wear characteristics was investigated. This was done by conducting three tests with increasing spiral cutting length while employing the same cutting conditions.

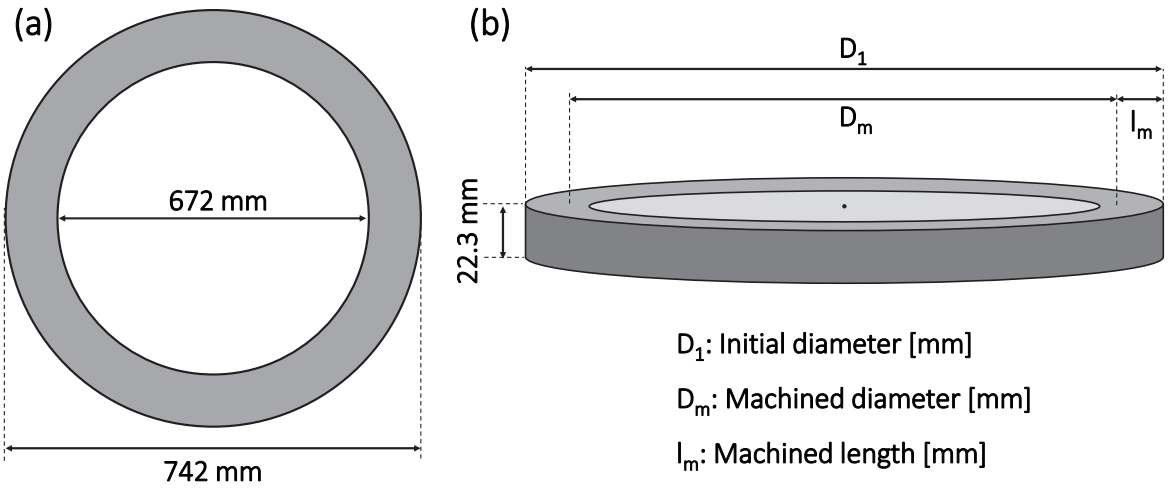

Figure 12: Dimension of the Alloy 718 workpiece used in the turning tests.

$$SCL = \left(\frac{D_1 + D_m}{2} \times \frac{\pi}{1000}\right) \times \frac{l_m}{f} \quad (1)$$

$$T_C = \frac{SCL}{v_c} \quad (2)$$

Table 2: Summary of conducted turning experiments. All tests were performed with high-pressure coolant supply of 16 MPa and 8 MPa to rake and flank face, respectively. Depth of cut was kept constant at 1 mm.

	Cutting speed, v_c [m/min]	Feed rate, f [mm/rev]	Tool type	Machined length, l_m [mm]	Spiral cutting length, SCL [m]
Paper 1	60	0.1	Conventional	25	565
	60	0.1	Surface-modified	25	565
	120	0.3	Surface-modified	25	70
Papers 2 and 3	60	0.2	Conventional	6.1	70
	60	0.2	Conventional	12.2	140
	60	0.2	Conventional	18.3	210

6.2 Coolant impingement tests

Coolant impingement and its influence on the tool surface was additionally investigated by subjecting tools to high-pressure cooling without machining at the same time. The used coolant supply pressures were the same as in the cutting tests (p_{Rake}=16 MPa and p_{Flank}= 8 MPa). Tests were conducted with increasing exposure times (1, 2, 5, 10, and 20 min).

6.3 Cutting tools

The characteristics of the used cutting tools are summarized in Table 3. Tests were done on tools in both conventional state (as-received) and after applying surface-modifications. In Figure 13, the conventional and the surface-midified tool are compared.

The surface-modifications were applied by laser machining (Sandvik Coromant) and consisted of arrangements of square pyramidal indents on both rake and flank faces. The first row of indents was placed at a distance of 0.2 mm and 0.1 mm from the cutting edge for the rake and flank side, respectively. The depth of the indents was increased with increasing distance from the cutting edge. Shallow indents in close vicinity to the cutting edge were used to avoid substantial weakening of the cutting edge. According to CAD calculations the overall surface area of the tool was increased by about 12% within the modified area. The intention of the surface modifications was to investigate whether an increase in contact area between tool and coolant can enhance the heat dissipation from the cutting zone and hence improve the tool life.

Table 3: Properties of the WC-Co tools used in the high-pressure jet assisted turning tests [48].

ISO code	RCMX 12 04 00 H13A
Coating	Uncoated
Inscribed circle diameter [mm]	12
Insert shape	Round
Face land width [mm]	0.2
Face land angle [°]	15
Clearance angle [°]	7

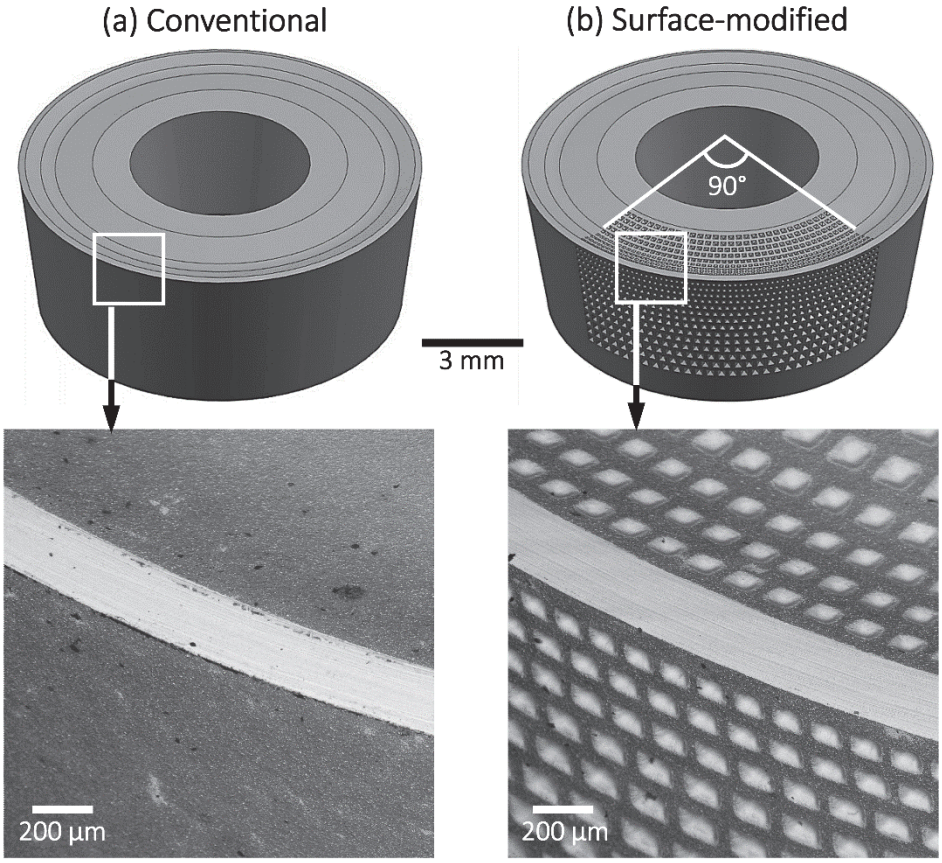

Figure 13: Illustrations of the tools and SEM micrographs of the cutting edges: (a) conventional tool; (b) surface-modified tool.

6.4 Sample preparation techniques

6.4.1 Removal of adhered workpiece layers

To characterize the worn tool surfaces in more detail, adhered layers of workpiece material were removed from the flank wear lands of selected tools. This was done by etching in HCl solution (50% HCl, 50% deionized water) at 75 °C. The etching time was increased stepwise while the etching-progress was checked by SEM. In order to avoid alterations of the wear characteristics by overetching, the etching time was kept as short as possible. Figure 14 exemplifies the results of the etching procedure: A layer of adhered workpiece material (dark) covering both rake and flank wear land (Figure 14a) was almost entirely removed after etching for 45 min (Figure 14b). As seen in Figure 14c, the etching procedure enables worn WC grains to be studied at higher magnification.

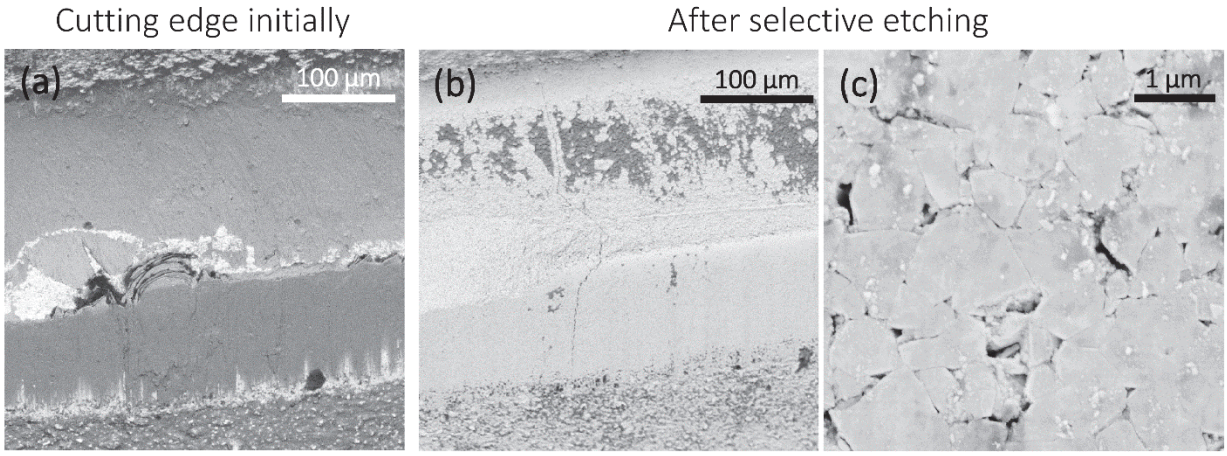

Figure 14: Removal of adhered material from worn cutting edge: BSE micrographs of cutting edge (a) prior and (b) after removal of the adhered layer by etching in HCl at 75 °C for 45 min. (c) SE image of the flank wear land at higher magnification.

6.4.2 Cross-sectioning by broad-ion-beam milling

A Leica EM TIC 3X ion milling system was applied to obtain cross-sections of the flank wear land including the adhered workpiece layer. Milling was conducted by the use of Ar ions with a beam energy of 6 keV.

6.4.3 Metallographic sample preparation

The workpiece microstructure was characterized on cross sections which were mounted in conductive resin followed by polishing with silica suspension. To reveal the microstructure, the samples were etched in a modified Kallings solution (1 g $CuCl_2$ in 50 ml methanol, 25 ml water, and 25 ml hydrochloric acid).

6.5 Characterization techniques

6.5.1 Scanning Electron Microscopy (SEM)

In SEM, electrons are emitted from an electron gun and subsequently focused onto the specimen by use of electric and magnetic lenses. The focused electron beam is scanned across the

specimen surface to be examined. The incident electrons interact with the atoms of the specimen leading to the formation of different types of radiation which can be used for imaging and analysis. Figure 15 shows the interaction of a primary electron beam with a specimen schematically.

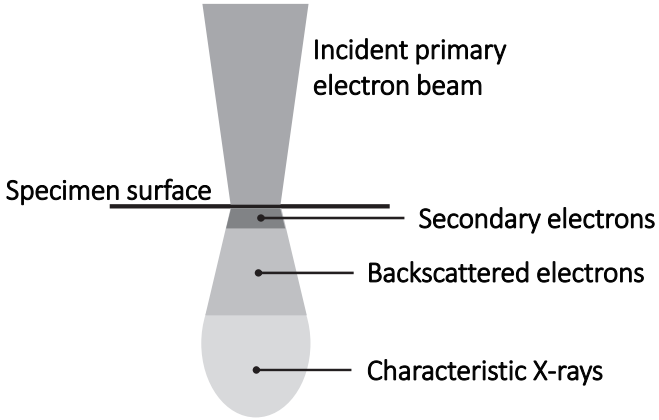

Figure 15: Interaction of an incident electron beam with specimen. Shown are some types of radiation emerging from the interaction volume which are commonly used for imaging and chemical analysis in SEM.

Secondary electrons (SE) are used for imaging topography while backscattered electrons (BSE) can be used for obtaining chemical contrast.

SE are outer shell electrons which are ejected from atoms of the specimen due to inelastic scattering of primary beam electrons. SE have low kinetic energy (< 50 eV), therefore only the SEs from comparably shallow depths are able to escape the specimen [49].

In contrast, BSE are electrons of the primary electron beam which have been scattered elastically. As they do not lose much energy, they can escape from deeper down of the specimen. Furthermore, the yield of BSEs is dependent on the atomic number of the elements in the probed specimen with heavy elements having higher yield than light elements. It is therefore possible to obtain chemical contrast with help of BSEs (heavy elements appear bright and light elements dark) [49].

The obtainable spatial resolution of SEM is dependent on the spot size of the focused electron beam as well as the size of the interaction volume which in turn is a function of the energy of the primary electron beam and the imaged material. Higher energy of the incident electrons and lower atomic number of the imaged material yield in a larger interaction volume.

In this study, a Leo 1550 Gemini SEM equipped with a field emission gun was used. Both BSE and SE were used for imaging.

6.5.2 Energy-dispersive X-ray spectroscopy (EDX)

The emission of characteristic X-rays by an incident electron beam is shown in Figure 16.

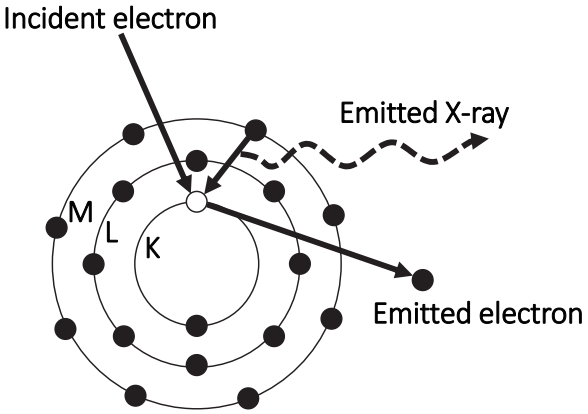

Figure 16: Schematic of emission of characteristic X-rays used for EDX.

The incident electron is scattered inelastically and leaves the atom ionized through emission of an electron of an inner shell. The inner vacant electron site can subsequently be filled by an outer shell electron and the atom returns to its ground state. In this way, its excess energy is released by releasing of an X-ray photon. The energy of the emitted X-ray is defined by the energy difference between the electron shells involved in the process. The energy of emitted X-ray photons is therefore characteristic for the electronic structure of the element. By detection and measurement of energies of emitted X-rays, it is therefore possible to obtain qualitative and quantitative chemical information of the specimen [49].

In this study, an EDX system with an Oxford X-Max silicon drift detector was used together with Aztec software for qualitative chemical analysis.

6.5.3 White-light interferometry

White-light interferometry (WLI), also referred to as coherence scanning interferometry, is an optical, non-contact method used to measure surfaces and their topographies in 3D. It extracts height information of the measured surface by analyzing interference patterns. The patterns are generated by superimposing light which was reflected from the sampled area with light reflected from a reference mirror. Details about the measurement principle can be found elsewhere [50].

In this study, the topography of the worn flank surfaces of the tools were studied using a MicroXAM instrument by ADE Phase shift Technologies. In Figure 17, an example WLI scan can be seen showing the topography of a worn flank face. The scan shows ridges which are oriented parallel to the workpiece sliding direction during cutting. Combination of such WLI scans with SEM can help to get a more comprehensive picture of wear patterns.

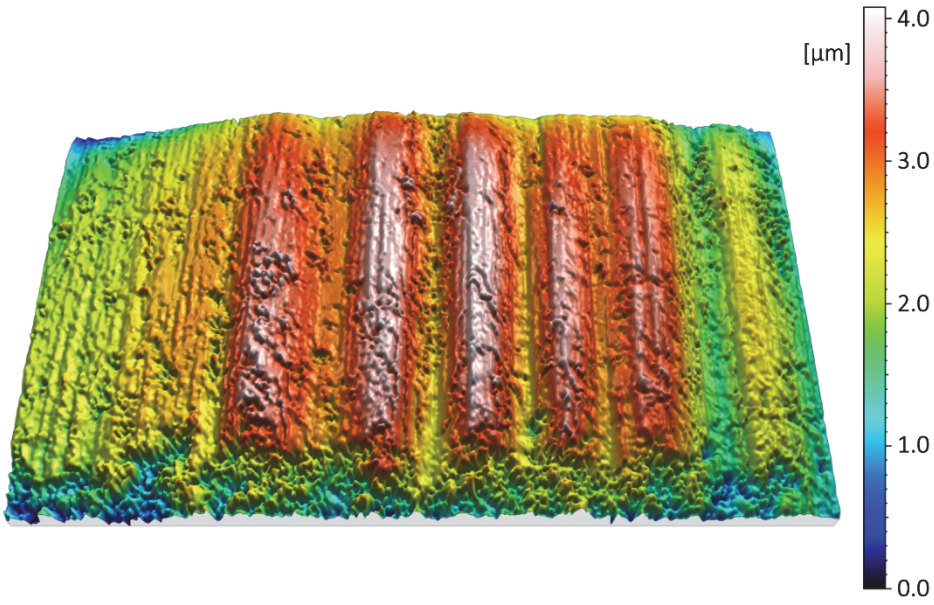

Figure 17: 3D contour map of an etched flank wear land obtained by white-light interferometry. The scanned area is 98 µm x 165 µm.

7 Summary of results and discussions

In order to address the objectives formulated in Chapter 1, the following three specific aspects were investigated:

(1) Influence of tool surface modifications on the wear behavior of the tools (Paper 1).
(2) Implications of the interaction of high-pressure coolant jets with the tool surface (Papers 2 and 3).
(3) Investigation of flank wear characteristics and of the influence of workpiece precipitates on the flank under sliding contact (Paper 3).

The following discussion and summary of the obtained results is structured in accordance to these aspects.

Combination of high-pressure cooling with tool surface modifications

The effect of surface-modifications on uncoated WC-Co tools in combination with high-pressure jet assisted machining was investigated in Paper 1. Obtained flank wear of a surface-modified cutting tool was compared to a conventional cutting tool (without surface-modifications) used for cutting Alloy 718 with the same cutting conditions (v_c = 60 m/min, f = 0.1 mm/rev, a_p = 1 mm) and coolant-supply pressures (p_{Rake} = 16 MPa and p_{Flank} = 8 MPa). As seen in Figure 18b, the flank wear land of the surface modified tool was reduced significantly as compared to the conventional tool (Figure 18a) after the same spiral cutting length of 565 m. Figure 18c provides a higher magnified micrograph of the flank wear land and the surface modifications. Furthermore, it was shown that the surface-modifications enable the tool to operate at a higher cutting speed (v_c = 120 m/min) and feed rate (f = 0.3 mm/rev) without sudden failure.

It was proposed that the reduction of flank wear can be associated to the increased surface area provided by the tool modifications. Specifically, enhanced coolant-tool interaction and better heat dissipation from the cutting zone leads to lower cutting temperatures. The tool material is therefore subjected to less thermal softening and can better withstand the imposed mechanical loads during cutting. Additionally, the surface-modifications allowed for higher cutting speeds and feed rates as compared to conventional tools.

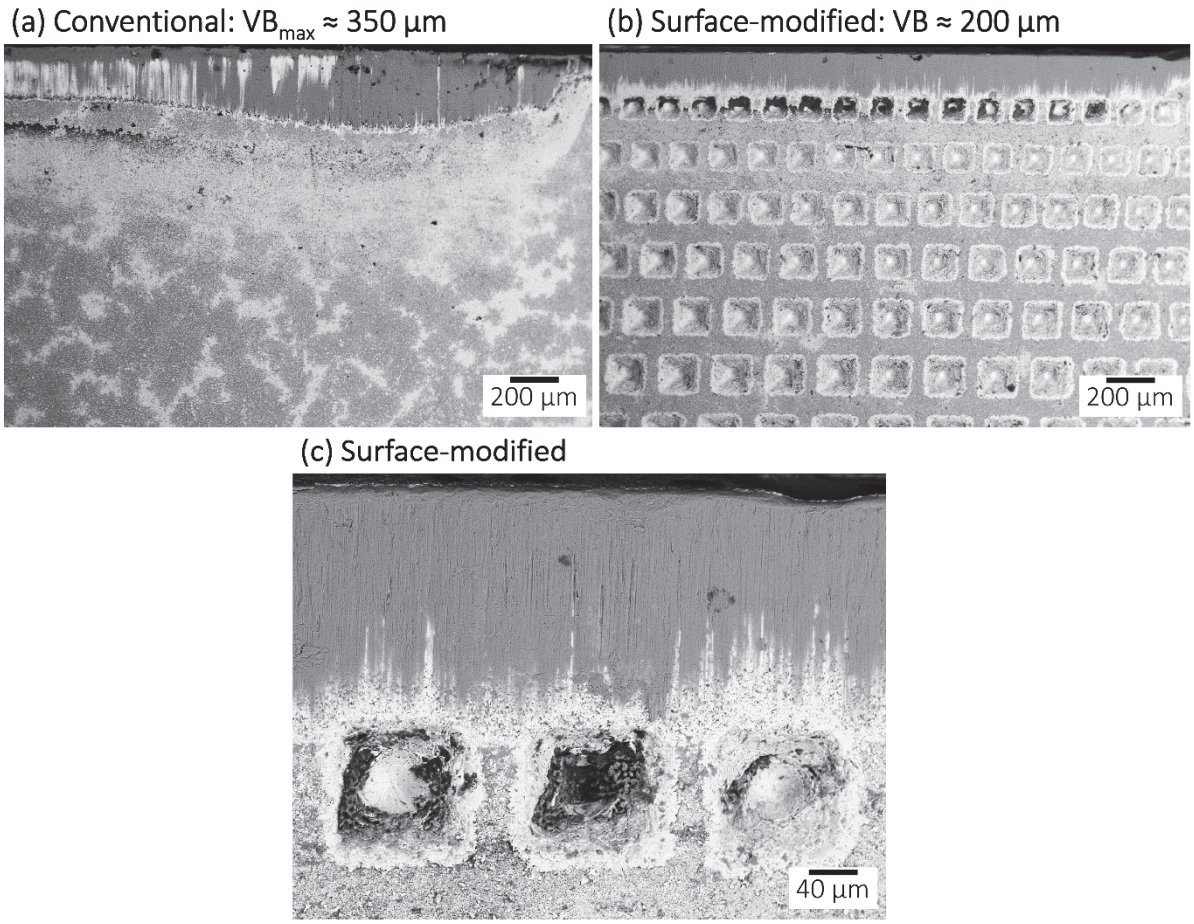

Figure 18: BSE micrographs of the obtained flank wear after high-pressure jet assisted machining for a spiral cutting length of 565 m: (a) conventional tool; (b) and (c) surface modified tool. Employed cutting parameters were v_c = 60 m/min, f = 0.1 mm/rev, a_p = 1 mm and coolant supply pressures were 16 MPa to rake face and 8 MPa to flank face, respectively.

Erosion by high-pressure coolant impingement

It was found that certain areas of the investigated tools are subjected to erosion. The erosion was connected to the impingement by the high-pressure coolant jets during machining. Erosion damage was confined to the Co-capping layer covering the uncoated WC-Co tool surfaces and was observed irrespective of the tool type (conventional or surface-modified). The extent of erosion damage of the Co-capping layer was spanning from sub-micron sized pits to complete removal.

In the coolant impingement tests without performing machining at the same time, it was found that the obtained erosion damage was by far less severe as compared to the machining tests (see BSE micrographs in Figure 19). This significant difference can be explained by the heat that dissipates into the tool from the shearing zones during cutting (see Figure 19b). The tool surface is therefore subjected to elevated temperatures and the Co is eroded more readily due to thermal softening.

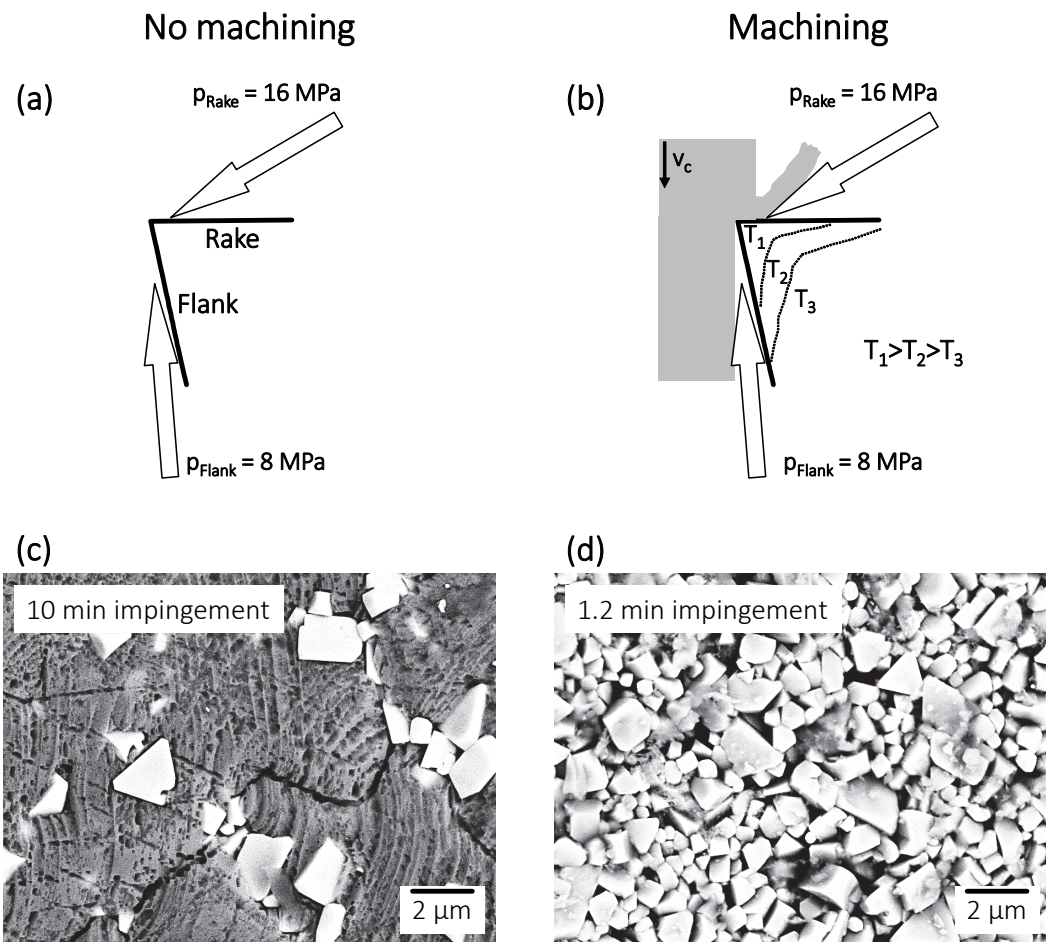

Figure 19: Illustrations of coolant impingement zones and BSE micrographs of the flank surfaces: (a and c) coolant impact without machining for 10 min; (b and d) coolant impact while machining for 1.2 min (v_c = 60 m/min, f = 0.2 mm/rev, a_p = 1 mm). Coolant jets are shown as arrows. Note the increase in temperature (T) due to heat generation in the shearing zones in (b).

Identifying the areas where erosion damage occurred during machining can give valuable information about the areas that were reached by the coolant, i.e. eroded during machining.

For the investigated cutting conditions, SEM observations lead to the conclusion that on the rake face the coolant reached all the way to the contact zone between chip and tool. On the flank face however, the coolant did not reach a zone close to the flank wear land as shown in Figure 20.

The differences between the locations of erosion on the rake face (erosion occurred all the way to the chip-tool contact zone) and flank face (erosion free zone close to the flank wear land) can be explained by the coolant supply pressures of 16 MPa and 8 MPa to rake and flank, respectively. The lower coolant supply pressure led to the formation of a vapor barrier (as described in Chapter 4) preventing the coolant from reaching closer to the cutting edge during cutting. Accordingly, higher supply pressures on the rake suppressed the formation of a vapor barrier.

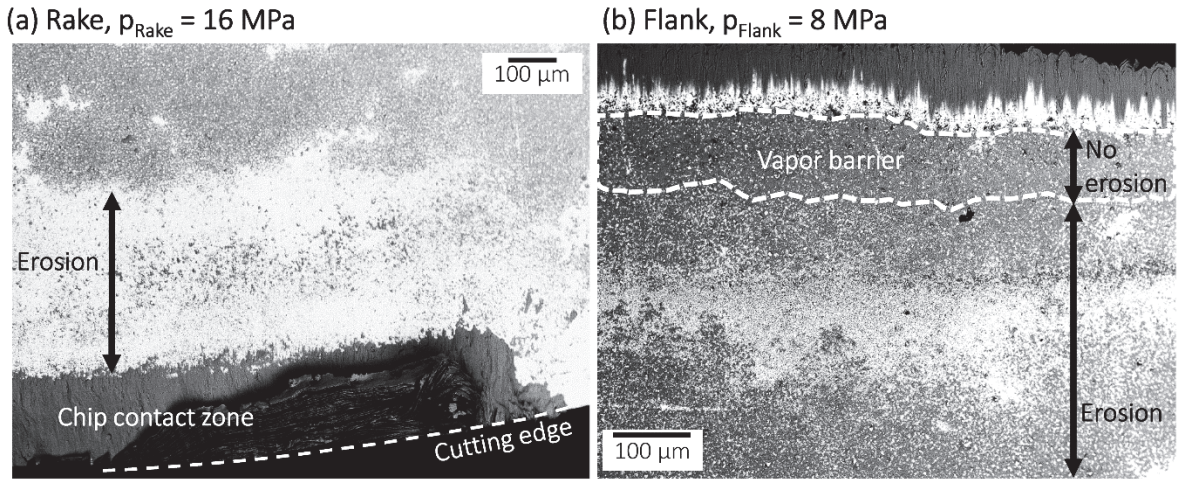

Figure 20: BSE micrograph of the worn and eroded tool surfaces: (a) rake face with erosion stretching all the way to the chip contact zone; (b) flank face with regions of erosion damage and vapor barrier (not eroded) indicated.

Flank wear mechanisms

The characteristics of flank wear obtained after cutting tests on Alloy 718 with increasing extent of wear (increased spiral cutting length of 70, 140, and 210 m) were analyzed in Paper 3. The flank wear lands were characterized by adhering workpiece material which made the underlying worn tool surfaces inaccessible for characterization. Removal of the adhered material was achieved by etching.

Subsequent SEM analysis revealed a scratch-free surface of the worn WC grains in the case of 70 and 140 m spiral cutting length. Locally, particles (sizes below 1 µm) were found to be left adhered to the WC grain surfaces despite the etching. EDX analysis of the adhered particles showed mainly presence of Nb which was assigned to the Nb-rich precipitates present in the workpiece (namely NbC and δ-phase).

As seen in Figure 21, when cutting with larger flank wear land (longer spiral cutting length of 210 m), the morphology of adhered fragments of precipitates changed to a smeared-out appearance.

This change was attributed to the increase in contact time between workpiece precipitates and the tool surface in the tertiary shearing zone during cutting. Furthermore, the thermal load in the tertiary shearing zone increases due to the larger contact area between tool and workpiece which gives rise to more frictional heat. This means that the workpiece precipitates are subjected to increased thermal loads which increases their ability to deform plastically. Increased plasticity together with the longer contact times explains the observed smeared-out appearance in connection with larger flank wear land.

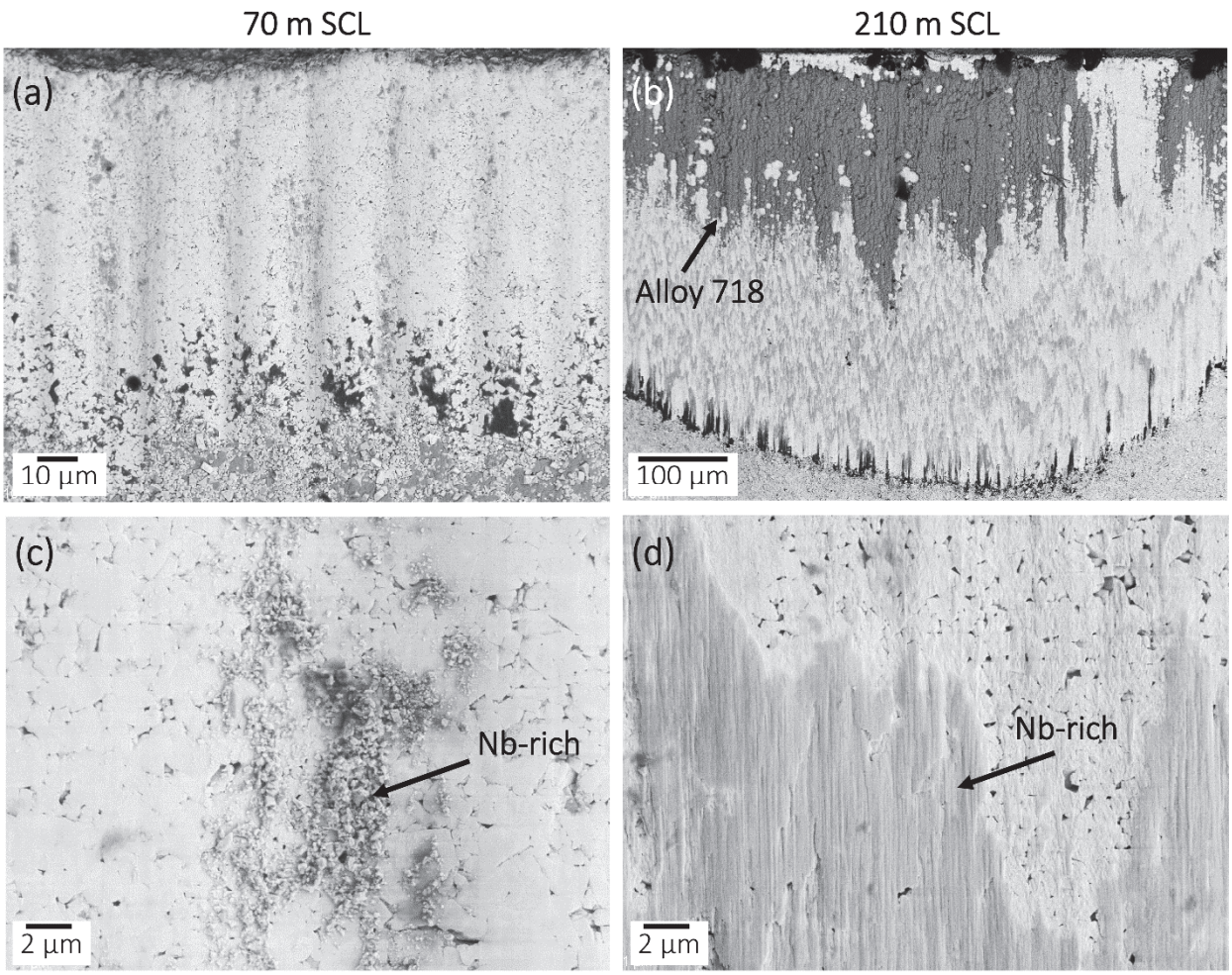

Figure 21: SEM micrographs of the flank wear lands after removal of adhered Alloy 718: (a and c) after short spiral cutting length; (b and d) after longer spiral cutting length. Notice the different flank wear widths.

Additional characterization of the tool microstructure beneath the flank wear land in cross-section showed plastic deformation by WC/WC grain boundary sliding within about 5 µm from the worn surface (see Figure 22). This was observed along the entire flank wear land. Additionally, fragmentation and elongation of individual WC grains was observed in close vicinity to the cutting edge. Hence, during cutting, the tool is subjected to the highest thermo-mechanical stresses in that region.

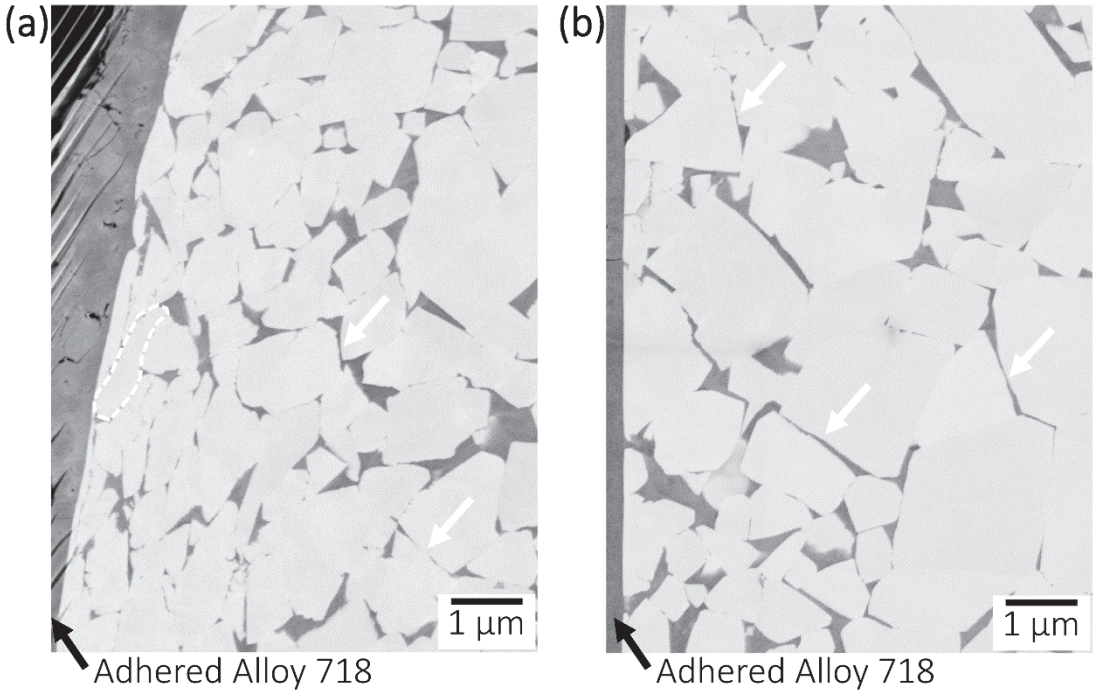

Figure 22: SEM micrographs of a flank wear land in cross section obtained by broad-ion-beam milling: (a) close to the cutting edge, (b) in the lower part of the flank wear land. Some grain boundaries subjected to sliding are marked by arrows and an elongated WC grain is encircled.

8 Future work

Erosion caused by the coolant-impingement and the possibility of investigating the vapor-barrier phenomenon was described in Paper 1 and 2. This opens up the possibility to study the effect of cutting parameters and coolant supply pressures on the vapor barrier and its location (i.e. coolant access to the cutting edge). This could help setting an optimal coolant supply pressure to avoid the vapor barrier phenomenon.

Coolant jets are subjected to a drop in pressure when propagating in air after exiting the nozzles (described in Paper 2). Quantification of this pressure-drop would enable to estimate the pressures at the vapor-coolant interface close to the cutting zone. As a consequence it would be possible to estimate the tool surface temperature from the vapor pressure of the coolant. Application of this method could be a valuable aid in understanding how cutting parameters and workpiece properties influence the thermal loads on the tools during machining.

Furthermore, the characterization approach taken in Paper 3 can be used to investigate the influence of chemical composition and microstructural aspects of different superalloys (e.g. different strengthening phases) on the obtained wear characteristics. This can help to explain the differing wear rates obtained when machining the respective alloys.

9 Acknowledgements

First of all I would like to thank my supervisor Prof. Uta Klement for giving me the opportunity to work with this subject as well as her guidance and support throughout this work.

Funding provided by Västra Götalandsregionen within the PROSAM project is highly acknowledged.

Furthermore I like to acknowledge my co-supervisor Prof. Tomas Beno and my twin PhD student Nageswaran Tamil Alagan, both at University West, for the collaboration and their contributions.

Anders Wretland and Dr. Stefan Cedergren, both GKN aerospace as well as Dr. Amir Malakizadi and Prof. Peter Krajnik, both Chalmers University of Technology are thanked for the inspiring discussions about metal cutting.

Furthermore, I would like to thank my friends and colleagues at the Department of Materials and Manufacturing Technology at Chalmers or the nice and inspiring working environment. A special thanks goes to Dr. Yiming Yao, Roger Sagdahl, Dr. Peter Sotkovszki, and Dr. Eric Tam for their help regarding practical work such as electron microscopy and metallography. Furthermore, I would like to thank Johanna Ekberg for being such a nice office mate.

Last but not least I would like to thank my family, relatives, and friends in Germany and around the world for being there for me.

10 References

[1] International Air Transport Association, "Economic Performance of the Airline Industry," 2016.

[2] The Boeing Company, "Current Market Outlook 2016-20135," Seattle, WA, 2016.

[3] R. E. Schafrik and R. Sprague, "Saga of gas turbine materials, part III," *Adv. Mater. Process.*, vol. 162, no. 5, pp. 29–33, 2004.

[4] J. H. Perepezko, "The Hotter the Engine, the Better," *Science*, vol. 326, no. November, pp. 1068–1069, 2009.

[5] Sandvik Coromant, "Application Guide - Heat resistant super alloys," 2010.

[6] R. C. Reed, *The Superalloys*, 1st ed. Cambridge: Cambridge Univ. Press, 2006.

[7] C. T. Sims, N. S. Stoloff, and W. C. Hagel, *Superalloys II*, 2nd ed. New York: Wiley-Interscience, 1987.

[8] G. F. Vander Voort, *ASM Handbook, Volume 09 - Metallography and Microstructures*. ASM International, 2004.

[9] "CES EduPack." Granta Design Limited, 2016.

[10] E. O. Ezugwu, J. Bonney, and Y. Yamane, "An overview of the machinability of aeroengine alloys," *J. Mater. Process. Technol.*, vol. 134, no. 2, pp. 233–253, 2003.

[11] I. A. Choudhury and M. A. El-Baradie, "Machinability of nickel-base super alloys: a general review," *J. Mater. Process. Technol.*, vol. 77, no. 1–3, pp. 278–284, May 1998.

[12] R. M'Saoubi, D. Axinte, S. L. Soo, C. Nobel, H. Attia, G. Kappmeyer, S. Engin, and W.-M. Sim, "High performance cutting of advanced aerospace alloys and composite materials," *CIRP Ann. - Manuf. Technol.*, vol. 64, no. 2, pp. 557–580, 2015.

[13] H. E. Exner, "Physical and chemical nature of cemented carbides," *Int. Met. Rev.*, vol. 24, no. 1, pp. 149–173, Jan. 1979.

[14] G. S. Upadhyaya, *Cemented tungsten carbides : production, properties, and testing*. Noyes Publications, 1998.

[15] F. Klocke, *Manufacturing Processes 1*. Berlin, Heidelberg: Springer Berlin Heidelberg, 2011.

[16] D. N. French and D. A. Thomas, "Crystallographic polarity of WC," *Anisotropy Single-Crystal Refract. Compd.*, pp. 55–66, 1968.

[17] G. S. Upadhyaya, "Sintering Behavior of Cemented Carbides," in *Cemented Tungsten Carbides*, 1998, pp. 138–165.

[18] D. Mari, *Mechanical Behavior of Hardmetals at High Temperature*, vol. 1. Elsevier Ltd, 2014.

[19] P. K. Wright and E. M. Trent, *Metal Cutting*, 4th ed. Woburn: Butterworth-Heinemann, 2000.

[20] G. S. Upadhyaya, "Mechanical Behavior of Cemented Carbides," in *Cemented Tungsten Carbides*, 1998, pp. 193–226.

[21] E. Rabinowicz, “Friction and Wear of Materials,” 1965.

[22] J. E. Stahl, *Metal Cutting Theories and Models*. Division of Production and Materials Engineering, 2012.

[23] Y. S. Liao and R. H. Shiue, “Carbide tool wear mechanism in turning Inconel 718 superalloy,” *Wear*, vol. 193, pp. 16–24, 1996.

[24] G. Östberg, K. Buss, M. Christensen, S. Norgren, H.-O. Andrén, D. Mari, G. Wahnström, and I. Reineck, “Mechanisms of plastic deformation of WC–Co and Ti(C, N)–WC–Co,” *Int. J. Refract. Met. Hard Mater.*, vol. 24, no. 1–2, pp. 135–144, 2006.

[25] G. Östberg and H.-O. Andrén, “Microstructural changes during wear by plastic deformation of cemented carbide and cermet cutting inserts,” *Metall. Mater. Trans. A*, vol. 37, no. 5, pp. 1495–1506, 2006.

[26] R. J. S. Pigott and A. T. Colwell, “Hi-Jet System for Increasing Tool Life,” Jan. 1952.

[27] E. O. Ezugwu and J. Bonney, “Effect of high-pressure coolant supply when machining nickel-base, Inconel 718, alloy with coated carbide tools,” *J. Mater. Process. Technol.*, vol. 153–154, pp. 1045–1050, 2004.

[28] E. O. Ezugwu and J. Bonney, “Finish Machining of Nickel-Base Inconel 718 Alloy with Coated Carbide Tool under Conventional and High-Pressure Coolant Supplies,” *Tribol. Trans.*, vol. 48, no. 1, pp. 76–81, 2005.

[29] A. R. C. Sharman, J. I. Hughes, and K. Ridgway, “Surface integrity and tool life when turning Inconel 718 using ultra-high pressure and flood coolant systems,” *Proc. Inst. Mech. Eng. Part B J. Eng. Manuf.*, vol. 222, no. 6, pp. 653–664, Jun. 2008.

[30] C. Courbon, D. Kramar, P. Krajnik, F. Pusavec, J. Rech, and J. Kopac, “Investigation of machining performance in high-pressure jet assisted turning of Inconel 718: An experimental study,” *Int. J. Mach. Tools Manuf.*, vol. 49, no. 14, pp. 1114–1125, Nov. 2009.

[31] F. Klocke, H. Sangermann, A. Krämer, and D. Lung, “Influence of a high-pressure lubricoolant supply on thermo-mechanical tool load and tool wear behaviour in the turning of aerospace materials,” *Proc. Inst. Mech. Eng. Part B J. Eng. Manuf.*, vol. 225, no. 1, pp. 52–61, 2011.

[32] H. Sangermann and F. Klocke, “Hochdruck-Kühlschmierstoffzufuhr in der Zerspanung,” Apprimus-Verl., 2013.

[33] R. Crafoord, J. Kaminski, S. Lagerberg, O. Ljungkrona, and A. Wretland, “Chip control in tube turning using a high-pressure water jet,” *Proc. Inst. Mech. Eng. Part B J. Eng. Manuf.*, vol. 213, no. 8, pp. 761–767, 1999.

[34] A. R. Machado and J. Walbank, “The Effects of a High-Pressure Coolant Jet on Machining,” *Proc. Inst. Mech. Eng. Part B J. Eng. Manuf.*, vol. 208, no. February, pp. 29–38, 1994.

[35] P. Dahlman, “A comparison of temperature reduction in high-pressure jet-assisted turning using high pressure versus high flowrate.,” *Proc. Inst. Mech. Eng. -- Part B -- Eng. Manuf. (Professional Eng. Publ.*, vol. 216, p. 467, 2002.

[36] J. Kaminski and B. Alvelid, “Temperature reduction in the cutting zone in water-jet assisted turning,” *J. Mater. Process. Technol.*, vol. 106, no. 1–3, pp. 68–73, Oct. 2000.

[37] K. Sørby and K. Tønnessen, “High-pressure cooling of face-grooving operations in Ti6Al4V,” *Proc. Inst. Mech. Eng. Part B J. Eng. Manuf.*, vol. 220, no. 10, pp. 1621–1627, 2006.

[38] A. W. Momber and R. Kovacevic, *Principles of Abrasive Water Jet Machining*. London: Springer London, 1998.

[39] K. Yanaida, “Flow Characteristics of Water Jets,” in *Second International Symposium on Jet Cutting Technology*, 1974.

[40] Dortmund Data Bank, “Vapor pressure of water,” 2017. [Online]. Available: www.ddbst.com. [Accessed: 02-Mar-2017].

[41] N. Kawasegi, H. Sugimori, H. Morimoto, N. Morita, and I. Hori, “Development of cutting tools with microscale and nanoscale textures to improve frictional behavior,” *Precis. Eng.*, vol. 33, no. 3, pp. 248–254, 2009.

[42] T. Sugihara and T. Enomoto, “Development of a cutting tool with a nano/micro-textured surface-Improvement of anti-adhesive effect by considering the texture patterns,” *Precis. Eng.*, vol. 33, no. 4, pp. 425–429, 2009.

[43] W. Chang, J. Sun, X. Luo, J. M. Ritchie, and C. Mack, “Investigation of microstructured milling tool for deferring tool wear,” *Wear*, vol. 271, no. 9–10, pp. 2433–2437, 2011.

[44] T. Obikawa, A. Kamio, H. Takaoka, and A. Osada, “Micro-texture at the coated tool face for high performance cutting,” *Int. J. Mach. Tools Manuf.*, vol. 51, no. 12, pp. 966–972, 2011.

[45] T. Enomoto, T. Sugihara, S. Yukinaga, K. Hirose, and U. Satake, “Highly wear-resistant cutting tools with textured surfaces in steel cutting,” *CIRP Ann. - Manuf. Technol.*, vol. 61, no. 1, pp. 571–574, 2012.

[46] T. Sugihara and T. Enomoto, “Improving anti-adhesion in aluminum alloy cutting by micro stripe texture,” *Precis. Eng.*, vol. 36, no. 2, pp. 229–237, 2012.

[47] T. Sugihara, “Performance of cutting tools with dimple textured surfaces: a comparative study of different texture patterns,” *Precis. Eng.*, 2017.

[48] Sandvik AB, “Product data.” [Online]. Available: http://www.sandvik.coromant.com/en-us/products/Pages/productdetails.aspx?c=rcmx+12+04+00+h13a. [Accessed: 17-Feb-2017].

[49] J. I. Goldstein, D. E. Newbury, P. Echlin, D. C. Joy, C. E. Lyman, E. Lifshin, L. Sawyer, and J. R. Michael, *Scanning Electron Microscopy and X-ray Microanalysis*. Boston, MA: Springer US, 2003.

[50] P. de Groot, “Coherence Scanning Interferometry,” in *Optical Measurement of Surface Topography*, Berlin, Heidelberg: Springer Berlin Heidelberg, 2011, pp. 187–208.